RSC Advances

ROYAL SOCIETY OF CHEMISTRY

www.rsc.org/advances

Journal Name

RSCPublishing

ARTICLE

Morphogenesis of ZnO nanostructures: Role of acetate ($COOH^-$) and nitrate (NO_3^-) ligand donor from zinc salt precursors in synthesis and morphology dependent photocatalytic properties

Cite this: DOI: 10.1039/xoxxoooooox

Received ooth January 2012,
Accepted ooth January 2012

DOI: 10.1039/xoxxoooooox

www.rsc.org/

Neeraj Kumar[a], Hemant Mittal[a], Leelakrishna Reddy[b], Padmanabhan Nair[b], Jane Catherine Ngila[a] and Vyom Parashar[a*]

We have studied the anions ratio effect of acetate and nitrate ions on the formation of different morphology of ZnO crystals in presence of NaOH and HMTA. We have varied the concentration of zinc salt precursors as well as adopted three different methods of synthesis (chemical, ultrasonic and hydrothermal) to study their effects on the size/shape of the formed ZnO nanostructures. We found that these anions which spontaneously get introduced along with zinc salt can modify the structure depending on their ratio. The photocatalytic properties of the as obtained ZnO nanostructures (nanoflower, nanospindle and nanorod) were tested towards anionic dye methyl orange. The results show that rod like ZnO nanostructures are catalytically more reactive than nanoflowers and nanospindles. Based on these results we propose that selection of appropriate zinc salt is significant to rationally design experiments for anticipated morphology. Furthermore, it is also suggested that role of other precursors salts in synergy will lead to formation of varied nanostructures and can be elaborated to other metal oxides of interest for modification.

Introduction

ZnO represents a material whose properties such as band gap, exciton binding energy, optical and electrical properties are strongly sensitive to morphology, size, aspect ratio, size orientation and crystal density[1-3]. These structural-characteristics-dependent fundamental properties of ZnO has led its applications towards lasers[4], light emitting devices[5], piezoelectric transducers[6], chemical sensors[7], solar cells[8], transparent electronics[9], and photocatalysts[10]. A variety of ZnO nanostructures (nanoflower[11], nanobelt[12], nanorod[13,14,16], nanosheet[14,16], nanotube[15], nanoribbon[16], nanowire[17] nanopyramid[10] and nanocrystal[10, 11, 16]) have been successfully developed by physical and chemical routes for example, vapor phase method, hydrothermal synthesis, microwave assisted solution reaction, spray pyrolysis, magnetron sputtering, pulsed laser deposition, molecular beam epitaxy and wet chemical route[2, 18-20]. However, compared to physical methods, solution phase methods have a clear superiority in terms of easy synthesis, flexibility, productivity and cost efficiency.

The formation of diverse shaped ZnO nanostructure predominantly rest on the relative surface energy of the crystal planes of the flourishing nanostructure [18, 21, 22]. ZnO crystals mainly have three crystal planes: a top polar zinc (0001) face, six symmetric nonpolar {1010} planes parallel to the [0001] direction, and a basal polar oxygen (0001) face. These different planes have different polarities (atomic arrangements) and are chemically distinct. Therefore, permutation and combination of different solvents, templates, surface capping agents and reaction conditions (such as pH, temperature etc.) generates various size and shape of ZnO nanostructures[23-28]. Moreover, it has been shown that introducing any growth modifiers (for example capping ligands) which have specific affinity towards any crystal face or surface can modify the relative growth rates and this modification reflects in the final crystal shape[23]. Though much attention and studies have been done in context of capping agents/different soft templates (surfactants[26], polymers[29, 31], di-block copolymers[30], citric acid[31], ascorbic acid[11] and amino acids[32]) but the effect of anions (NO_3^-, $COOH^-$, Cl^- etc.) which get introduced when any zinc salt is used in the reactions is not consolidated.

Therefore, we sought to investigate the effect of two different salts of zinc (acetate and nitrate) on crystal formation when introduced together in the reaction at different ratio in aqueous media. We also involved two different alkaline sources (NaOH and HMTA) expanding the investigation further by

Table 1

Concentration ratio (mM) Zinc Acetate : Zinc Nitrate	Time (h)	Reaction methods and morphology					
		Chemical route[a]		Ultrasonication[b]		Hydrothermal[c]	
		$ChemR^{NaOH}$ (pH = 8)	$ChemR^{HMTA}$	$SonicR^{NaOH}$ (pH = 8)	$SonicR^{HMTA}$	$HydroR^{NaOH}$ (pH = 8)	$HydroR^{HMTA}$
0:10	5	Nanoflower	Nanoneedle	Nanoflower	Nanorod	Nanosheet-Flower	Nanorod
5:5	5	Nanoflower	Nanorod	Nanospindle	Nanorod	Irregular nanosheet	Distorted Nanorod
10:0	5	Spherical aggregate	Nanoneedle	Nanoflower	Nanorod	Spherical aggregate	Nanorod

HMTA (hexamethylene tetramine), [a]Temperture = 80 °C, [b]Temperture = room temperature, [c]Temperture = 120 °C.

adopting three different solution phase methods (chemical, ultrasonic and hydrothermal). Furthermore, the present article embarks on the following questions: What effect do different salt precursors of zinc have with changing ratio in defining the final morphology? How does changing the reaction conditions with changing different salts ratio affects the final morphology? After these investigations have been achieved, we embark on one more interesting objective, that is: with different morphology thus obtained which nanostructure is imperative for exploring the full potential as a photocatalyst? Previous studies showed that photocatalysis is an important application of ZnO nanostructures for environmental pollution remediation[10, 33]. Low dimensional nanostructures have higher tendency to promote the photo-generated charge carriers due to an increased delocalization of electrons[33 -35]. Therefore, the question of different nanostructures based photo-catalysis performance becomes interesting.

Experimental

Chemical and reagents

All of the analytical-grade reagents were purchased commercially and used as received. One molar aqueous solution of zinc acetate dihydrate (98% purity, Sigma Aldrich), zinc nitrate hexahydrate (98% purity, Sigma Aldrich), HMTA Hexamethylenetetramine (99.99% purity, Sigma Aldrich) and NaOH (97% Sigma Aldrich) were prepared in stock, separately.

Synthesis of zinc oxide nanostructures

Three different methodologies were adopted to fabricate ZnO nanostructures *viz.* chemical method, hydrothermal method and ultrasonic method. For each mentioned methods we performed two sets of reactions, one in presence of NaOH and second in presence of HMTA. To avoid the confusion in discussion of the results these reactions were named as $ChemR^{NaOH}$ and $ChemR^{HMTA}$ (for chemical method), $HydroR^{NaOH}$ and $HydroR^{HMTA}$ (for hydrothermal method) and $SonicR^{NaOH}$ and $SonicR^{HMTA}$ (for ultrasonic method). Moreover, for all the above reactions (*viz.* $ChemR^{NaOH}$, $ChemR^{HMTA}$, $HydroR^{NaOH}$, $HydroR^{HMTA}$, $SonicR^{NaOH}$ and $SonicR^{HMTA}$) were executed using zinc acetate and zinc nitrate salt with varying millimolar (mM) ratio of both the salt precursors (Zn^{2+} $_{Acetate\ salt}$: Zn^{2+} $_{Nitrate\ salt}$; 0: 10, 5: 5, and 10: 0) to elucidate the morphological evolution of ZnO nanostructures. In brief, for $ChemR^{NaOH}$ reaction different millimolar ratios of Zn^{2+} $_{Acetate\ salt}$: Zn^{2+} $_{Nitrate\ salt}$ (as mentioned above) were dissolved in 100 ml deionized water. Further, pH of each solution was adjusted to 8.0 using 1 M solution of NaOH. Then, reaction mixture was stirred at 80 °C for 5h. For $ChemR^{HMTA}$ all reaction conditions were same as of $ChemR^{NaoH}$ except that 10 mM HMTA was introduced in all the reactions instead of NaOH. Similarly, $HydroR^{NaoH}$ and $HydroR^{HMTA}$ reactions were performed with the difference that each prepared solution was transferred to a teflon-lined autoclave and then maintained at 120 °C for 5 h. Similarly, for $SonicR^{NaoH}$ and $SonicR^{HMTA}$ reactions each prepared solution was transferred into an ultrasonic bath at room temperature for 5 h. For all the reactions mentioned above the resultant white precipitate was centrifuged and washed thrice with deionized water and finally with absolute ethanol. Samples were dried at 60 °C for overnight. All the reactions set-up and conditions has been summarized in Table 1.

Photocatalytic Activity

All photocatalysis experiments were carried out under identical conditions using a representative of an anionic azo dye, methyl orange (MO) as test contaminant. A 12 ppm solution of MO was prepared in deionized water in which 40 mg of ZnO nanostructures as catalysts were suspended. The photocatalytic activities were evaluated by the photodegradation of MO under UV light irradiation with a light irradiation system containing an Hg-lamp in dark chamber at room temperature. The distance between dye solution and lamp was kept 5 cm. Prior to illumination of UV light, the solution was magnetically stirred in the dark for 30 min to attain an adsorption–desorption equilibrium. At regular intervals, optical absorption spectra were recorded using an UV−vis spectrophotometer in order to monitor the rate of photodegradation by analyzing the reduction in the absorption intensity of MO at a maximum adsorption peak at 463 nm (λ_{max} for MO). The time course of the photocatalytic degradation of MO was also determined to

understand the photocatalytic stability of the ZnO nanostructures.

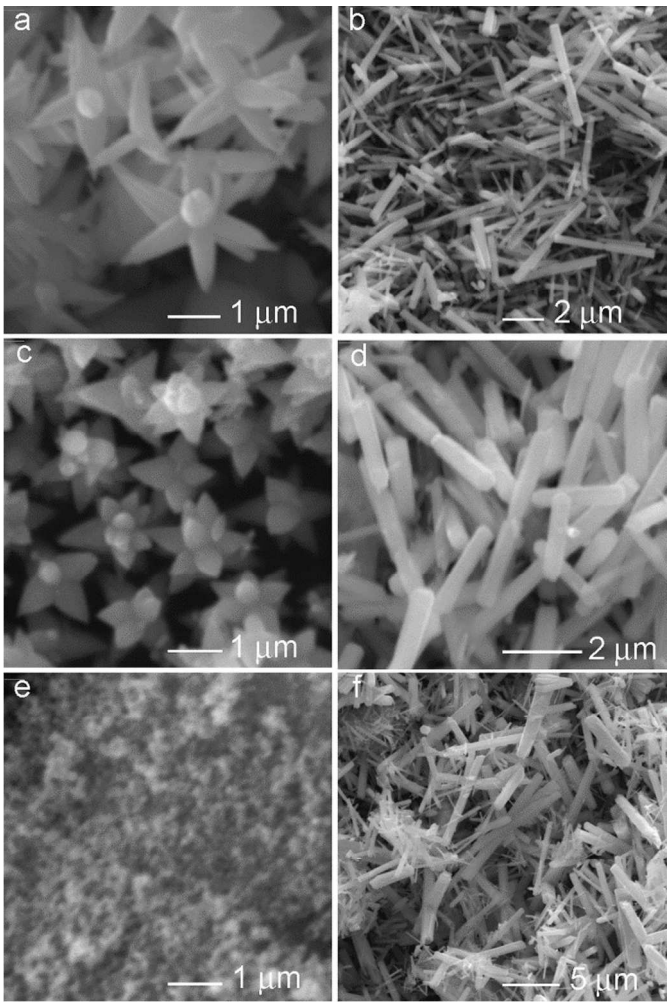

Fig 1. SEM images of ZnO nanostructures are grown via simple chemical route under ChemR^{NaoH} (a, c and e) and ChemR^{HMTA} (b, d and f). The images (a, b), (c, d) and (e, f) are corresponding to zinc acetate/zinc nitrate ratio 0:10, 5:5, and 10:0 respectively.

Results and discussion

We divided the anion-related (acetate and nitrate ions) ZnO nanostructure evolution into three groups according to the method adopted to synthesize ZnO. Group A contained chemical method, Group B contained ultrasonic method and Group C contained hydrothermal method. For all the three groups reactions has been performed in two sets, one in presence of NaOH and second in presence of HMTA. An alkaline solution is essential for the formation of ZnO nanostructures because normally divalent metal ions do not hydrolyze in acidic environments[36]. NaOH is the most widely used alkaline source for ZnO formation. Furthermore, it has been suggested that Na^+ forms a virtual capping layer around the nanocrystal thus inhibiting the nanocrystal growth[37]. Moreover, the concentration of OH^- determines the size and growth rate of ZnO nanostructures. Also it is suggested that pH value of solution has a complex relationship with OH^- concentration and increasing pH values increases the growth rate however increasing beyond 10 tend to lower this rate[38]. Though, it occurs

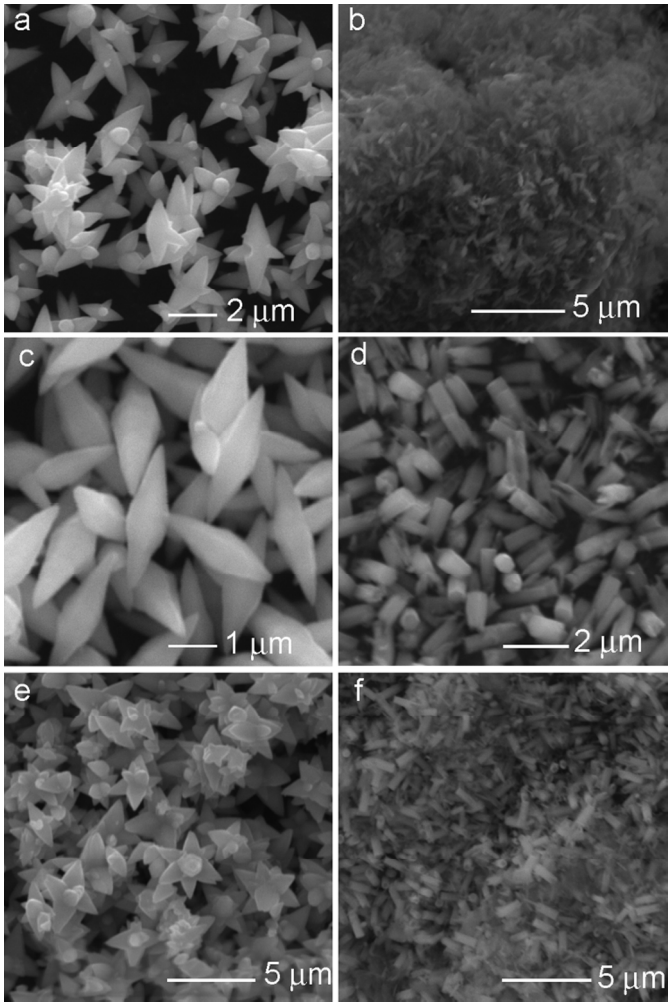

Fig 2. SEM images of ZnO nanostructures are grown via ultrasonication under SonicR^{NaoH} (a, c and e), SonicR^{HMTA} (b, d and f). The images (a, b), (c, d) and (e, f) are corresponding to zinc acetate/zinc nitrate ratio 0:10, 5:5, and 10:0 respectively.

that researchers agree on the role of NaOH, as a matter of fact there is not a general consensus on the precise role of HMTA despite the fact that a number of papers have been published since its first utilization 30 years ago[39]. Among so many papers on the role of HMTA, study conducted by Sugunan *et al*. and McPeak *et al*. are very interesting as they contradict[40, 41]. Sugunan *et al.* proposed that HMTA preferentially attaches to the nonpolar facets of ZnO acting as a nonpolar chelating agent. This induces anisotropic growth along the c-axis. However, McPeak *et al.* refuted this mechanism and proposed that the role of HMTA is only to control the saturation index of ZnO through the slow release of OH^- ions. Recently, Vincenzina *et al.* proposed that HMTA plays a dual role participating both as supplier of OH^- and as capping agent promoting anisotropic growth[42].

Interestingly a lot has been investigated on the role of alkaline source, capping ligand and physical parameters (pH, temperature etc.). However, there is a lack of consolidated and systematic information on the role of anions which are very much present and come along with zinc salts being used as precursors. We investigated how the presence of one anion effects the overall ZnO growth in the presence of another anion. We found that the presence of two anions do effect the ZnO growth and morphology and change with changing reaction conditions, as shown in Table 1. We have restrained ourselves from elucidating reaction equations as to precisely conclude the reaction equation a high-resolution solid-state NMR measurements are needed and seeing the number of reactions involved it is not feasible for the present article. However, we left this question for future investigation and focused on the dynamics of anions and ZnO morphology evolving out of this.

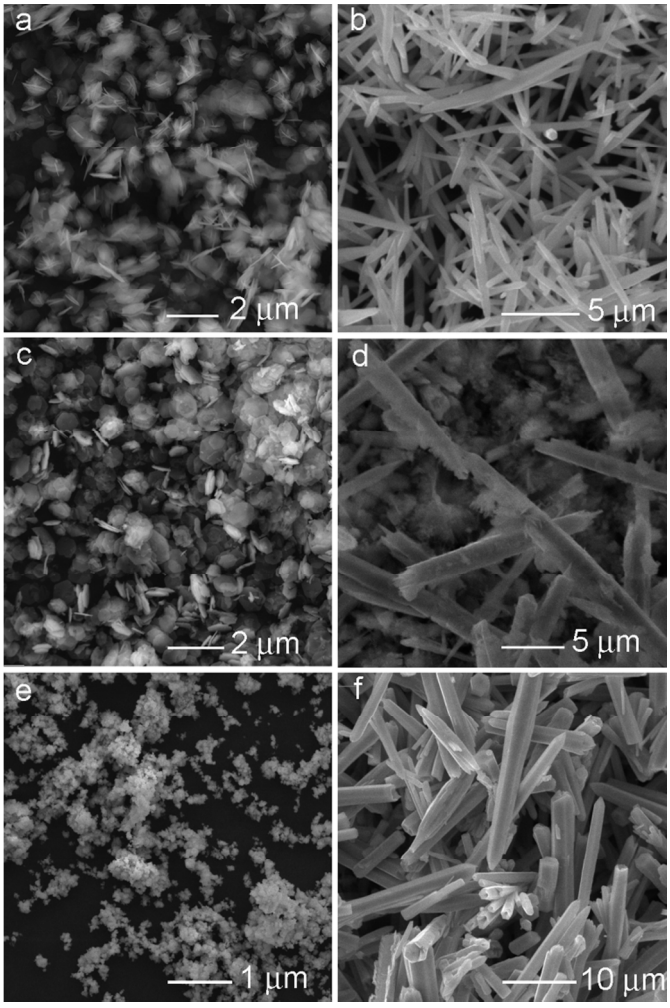

Fig 3. SEM images of ZnO nanostructures are grown via hydrothermal method HydroR^{NaoH} (a, c and e) and HydroR^{HMTA} (b, d and f). The images (a, b), (c, d) and (e, f) are corresponding to zinc acetate/zinc nitrate ratio 0:10, 5:5, and 10:0 respectively.

Effect of anions on ZnO crystal formation *via* simple chemical method (Group A)

SEM images of ZnO nanostructures grown via simple chemical method are shown in figure 1. The images (a, c and e) represent morphologies grown under ChemR^{NaOH} and images (b, d and f) shows morphologies obtained under ChemR^{HMTA}. The images (a, b), (c, d) and (e, f) are corresponding to zinc acetate/zinc nitrate millimolar ratio 0:10, 5:5, and 10:0 respectively. Figure 1a for zinc acetate/zinc nitrate millimolar ratio 0:10 clearly shows the formation of flower shaped ZnO nanostructures, whereas Figure1e shows spherical morphology for zinc acetate/zinc nitrate milli-molar (mM) ratio of 10:0. Interestingly, Figure 1 b, d and f show formation of nanorod with varying aspect ratio.

During ChemR^{NaOH} reaction in the presence of only nitrate ligand, as shown in Figure 1 a, ZnO structure evolved into flower shape. Because the initial ZnO seed has multiple polar (0001) surfaces and factually, nonpolar {1010} has lower surface energy and are more stable than polar planes the system tends to minimize the total surface energy, ZnO crystal spines grow along the [0001] direction forming flower shape. Furthermore, studies have shown that in the presence of ligands (for example ascorbate ligand or PEG) which has many oxygen atoms $Zn(OH)_4^{2-}$ growth units were adsorbed by the O atom and the fast crystal growth rate of ZnO resulted in the formation of flower like shape[11, 43]. In this case nitrate ion has three oxygen atoms available. It seems that presence of at least three oxygen atoms is a vital parameter for growth of ZnO crystal to flower shape because we observed spherical aggregates or particle growth in the presence of acetate ligand which has only two oxygen atoms (Figure 1e). Figure 1e results further suggests that the stabilization effect of the surface by acetate ligands on $Zn(OH)_4^{2-}$ growth units probably depress the straightforward growth of ZnO, leading to spherical particles[44]. Figure 1c for zinc acetate/zinc nitrate millimolar ratio 5:5 demonstrates the same results as Figure 1a with only difference in the width of the spines increased. This is probably due to the synergistic behavior of nitrate and acetate ions. However, Figure 1 c demonstrates the dominance of nitrate ions over acetate ions in controlling the final shape of ZnO crystal to flower shape. This result further suggest that using acetate salts will tend to give much smaller particle of uniform diameter compared to nitrate salts due to low decomposition temperature.

Figure 1b and 1f for zinc acetate/zinc nitrate millimolar ratio 0:10 and 10:0 respectively show that ZnO merges as nanoneedles form of varied aspect ratio in the presence of HMTA (ChemR^{HMTA} reaction). However, for zinc acetate/zinc nitrate millimolar ratio 5:5 we observed uniform nanorod. These results suggest that HMTA is the main controlling factor in determining the final shape of ZnO. However, with equal ratio of acetate and nitrate ligand a more controlled growth occurs. Therefore, the role of both anions in forming the homogeneous nanorod cannot be ruled out. These results further supports the observation of Vincenzina *et al.*[42] that HMTA plays a double role, acting as pH regulator, and induces the vertical growth of ZnO nanorod along the c-axis.

Effect of anions on ZnO crystal formation *via* ultrasonication method (Group B)

SEM images of ZnO nanostructures grown *via* ultrasonication method are shown in figure 2. The images (a, c and e) represent morphologies grown under SonicR^{NaOH} and images (b, d and f) shows morphologies obtained under SonicR^{HMTA}. The images (a, b), (c, d) and (e, f) are corresponding to zinc acetate/zinc nitrate

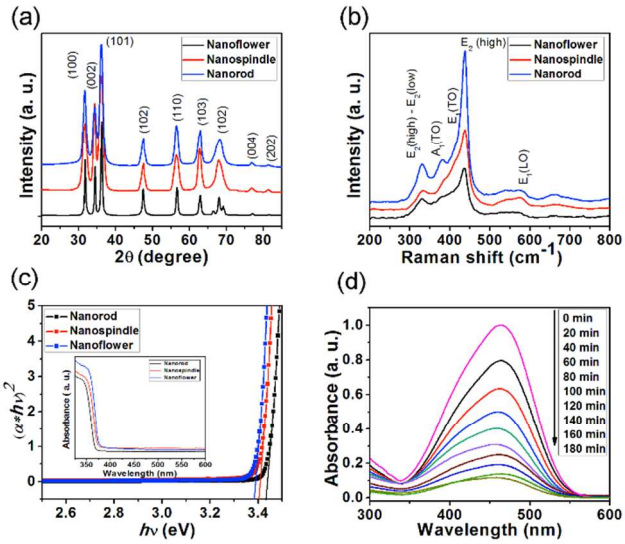

Fig 4. (a) and (b) XRD and Raman spectra of different ZnO nanostructures (nanoflower, nanorod, nanospindle), respectively; (c) the plot of $(\alpha h\nu)^2$ versus $h\nu$ for ZnO nanostructures and inset shows the corresponding UV-vis absorption spectra; (d) UV-visible absorbance spectra of photodegradation of MO in the presence of ZnO nanostructures

millimolar ratio 0:10, 5:5, and 10:0 respectively. Figure 2 a for zinc acetate/zinc nitrate millimolar ratio 0:10 clearly show the formation of flower shaped ZnO nanostructures as were observed in Figure 2a for ChemR^{NaOH} reaction. Interestingly for zinc acetate/zinc nitrate millimolar ratio 10:0 we still observed the flower shaped ZnO which is different from what we observed in Figure 1 e for ChemR^{NaOH} reaction. This change of morphology (from agglomerated spherical nanoparticles to flower shaped) can be attributed to the ultrasound radiation. It can be clearly noticed that there is first formation of spindle structure, and then it grows as emerging budding like shape as partially grown flower and finally convert into complete flower. These flowers actually form with a central spindle and a few half spindles pointing outward that appear as the petals of a flower initiating from center of the half spindle (shown in figure 2a). The sonication process comprises the formation, growth and collapse of bubbles that can break the chemical bonds of materials in an aqueous medium. Sonication process generates two possibilities: 1) this condition induces the quantum confinement effect (or formation of multi-polar surface) by rupturing the agglomeration and thus increasing the chemical activity. This results in the ZnO crystal spines growth along the [0001] direction forming flower shape. 2) The ultrasonic radiation accelerates the chemical reaction between the surface of the anions and cations[45]. In particular, the ultrasonic radiation causes cavitations around the surface of the ZnO seed and heating of the precursor solution. As the cavitations collapse near the surface of the ZnO seed, the shock waves cause effective mixing of the precursor solution, resulting in a fast diffusion of hydroxyl ions on the surface of the ZnO seed[46]. Thus limiting the stabilizing effect of acetate ions as was observed in ChemR^{NaOH} reaction for Figure 1e. Though we observed flower shaped ZnO formation when acetate and nitrate ligands perform independently in the presence of NaOH under sonication we observed a totally different spindle like morphology for zinc acetate/zinc nitrate millimolar ratio 5:5. This again suggests that presence of two different anionic ligands in the reaction can alter the morphology and has controlling effect on the growth kinetics and direction. The role of two anions in creating different morphology presents a new perspective on formation of new morphology. Moreover, it will be interesting to see how morphology evolves when three or more anions ligands (or zinc salts) are introduced in the reactions adopting different methodology.

During the SonicR^{HMTA} reaction the role of HMTA is still the main controlling factor giving rod shape morphology as evident from Figure 2 b, d and e. Compared to ChemR^{HMTA} reaction sonication process has decreased the aspect ratio of the nanorod for all the anion ligand ratios. For zinc acetate/zinc nitrate millimolar ratio 5:5 (Figure 2 d) semi-porous nanorod was formed. This shape transformation can be explained in terms of the difference in the growth rates of various crystal faces in the presence of acetate and nitrate ligands[47]. This may expedite the formation of the ZnO semi hollow nanorod as thermodynamic will dominate the reaction under ultrasonic radiation. Furthermore, we also suspect the role of acetate ligand in making such semi hollow nanorod as we observed the similar structure in HydroR^{HMTA} reaction (Figure 3 f) for zinc acetate/zinc nitrate millimolar ratio 10:0. This might be due to the interplay of lower energy (of acetate ligand) on hollow side and high energy (of nitrate ligand) on polar surfaces[15, 48].

Effect of anions on ZnO crystal formation *via* hydrothermal method (Group C)

SEM images of ZnO nanostructures grown via hydrothermal method are shown in Figure 3. The images (a, c and e) represent morphologies grown under HydroR^{NaOH} and images (b, d and f) show morphologies obtained under HydroR^{HMTA}. The images (a, b), (c, d) and (e, f) are corresponding to zinc acetate/zinc nitrate millimolar ratio 0:10, 5:5, and 10:0 respectively. For molar ratio of zinc acetate/zinc nitrate 0:10 (Figure 3a) nanosheets-assembled hierarchical flower-like ZnO nanostructures formed[49].

In the presence of both acetate and nitrate ions, nanosheets with some irregularities were obtained. Whereas for molar ratio of zinc acetate/zinc nitrate 10:0 (Figure 3 e) spherical aggregates of nanoparticles can be seen. There are reports where ZnO sheets have been fabricated using zinc acetate via hydrothermal or reflux methods[16, 50]. However, all these

experiments were performed in the presence of capping agent or additive. Liu *et. al*.[50] has presented a probable mechanism for sheet formation with zinc acetate. They suggest that under alkaline conditions layered basic zinc acetate clusters are generated. These layered clusters induce ZnO nanoparticles to attach to the laminar surface through acetate anions thus forming sheets. However, we noticed that they performed this reaction in ethylene glycol solvent. The

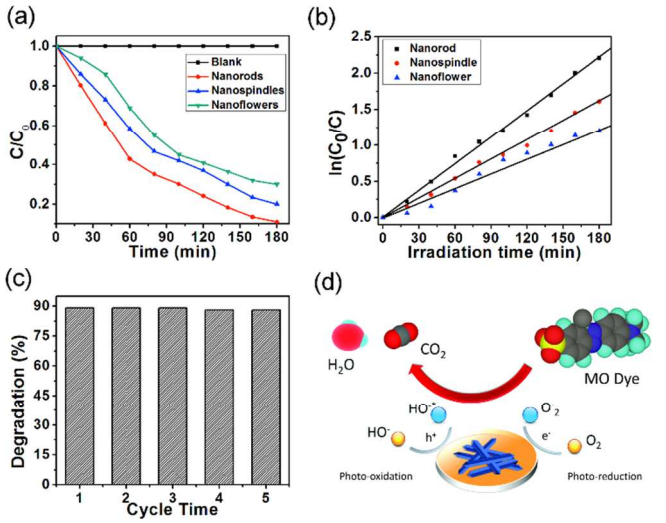

Fig. 5 (a) Photocatalytic activity for the degradation of MO solution by using different ZnO nanostructures photocatalyst under UV light irradiation; (b) The kinetic relationship of ln(C/C0) vs. irradiation time curves; (c) The stability of ZnO nanorod for photodegradation of MO; (d) Schematic representation of photocatalytic process in the presence of ZnO nanostructures.

role of ethylene glycol cannot be ruled out. This is the reason that probably we didn't see sheet like morphology for molar ratio of zinc acetate/zinc nitrate 10:0 (Figure 3 e). Moreover, for zinc acetate/zinc nitrate millimolar ratio 5:5 we observed irregular nanosheets (Figure 1c). We anticipate that under hydrothermal condition the dynamic of acetate and nitrate anions did not worked out well as compared to other cases.

During the HydroR^{HMTA} reaction for zinc acetate/zinc nitrate millimolar ratio 0:10 we observed well crystalline nanorod. The role of HMTA is well documented for fabricated nanorod and also been discussed in previous sections. Interestingly, for zinc acetate/zinc nitrate millimolar ratio 5:5 though nanorod was formed but they are not smooth compared to what we observed for Figure 1d (ChemR^{HMTA}). Probably under hydrothermal condition the dynamic of both the anions did not worked out well as compared to above cases. However, for zinc acetate/zinc nitrate millimolar ratio 10:0 we observed semi hollow nanorod with high aspect ratio. Under HydroR^{NaOH} probably acetate anions interact with Zn^{2+} on ZnO nanoparticles causing lowering of the surface energy and attaining a metastable intermediate[15, 48] similar to what we observed for SonicR^{HMTA} (Figure 2 d). The only difference is of high aspect ratio which can be interpreted by high thermodynamics under hydrothermal conditions[47].

Characterization

For XRD, Raman, UV absorption characterization and photocatalytic properties we selected flower shaped ZnO nanostructure from Group A (Figure 1c), spindle shaped ZnO from Group B (Figure 2 c) for zinc acetate/zinc nitrate millimolar ratio 5:5. As evident nanorod are formed in each group with varying aspect ratio. Moreover, for zinc acetate/zinc nitrate millimolar ratio 5:5 ratio we didn't observe sample homogeneity therefore we chose sample (Figure 3b) as a representative for nanorod based on high aspect ratio for photocatalytic performance.

Figure 4a represents XRD patterns of ZnO for each group. All the diffraction peaks are in good agreement with standard data JCPDS no. 89-1397. It can be clearly noticed that pattern of all peaks showed a single phase nature with a hexagonal wurtzite structure of ZnO.

Figure 4b represents the Raman spectrum of nanoflower (Group A), nanospindle (Group B) and nanorod (Group c). The spectrum shows conventional vibrational modes of E_2 (high) – E_2 (low), A_1(TO), E_1(TO), E_2(high) and longitudinal optical mode E_1(LO). The nonpolar Raman active modes E_2 (high) and E_2(low) have been assigned to oxygen atoms or vibrations and Zn sub-lattice[51]. The Raman peaks centered at 381cm^{-1}, 408 cm^{-1}, 437 cm^{-1}, and 577 cm^{-1} were attributed to the A_1(TO), E_1(TO), E_2(high) and E_1(LO) Raman modes of the wurtzite phase of ZnO, respectively[3]. It can be clearly observed from figure 4b that the intensity of E_2(high) becomes weaker on shifting from nanorod to nanoflower nanostructures, which shows the more intrinsic defects associated with O atoms. The high intensity of E_2(high) mode for nanorod nanostructures occurred due to increase in supersaturation[52]. However, there was no change noticed in the intensity of E_1(LO) mode for all the samples. It is noteworthy that normally forbidden E_1(LO) mode has activate for these nanostructures, which indicate pronounced enhancement of the surface activity compared with that of the bulk crystals with large surface area and high surface roughness.

Figure 4c represents the optical absorption spectra for nanoflower (Group A), nanospindle (Group B) and nanorod (Group C) respectively. The absorption spectrum for each group representative is shown in inset figure 4c. The absorption spectrum of nanoflower is shifted to shorter wavelength but for nanospindle and nanorod, the absorption band is shifted towards higher wavelength with high intensity. These results indicated that the aspect ratio of the ZnO nanostructures leads to the corrections in the energy bands causing the band gap tuning. The band gap energy of different nanostructures of ZnO was calculated using the following formula[53]:

$$(\alpha h\nu) = A(h\nu - E_g)^{1/2} \qquad (1)$$

where α, h, ν, E_g and A are absorption coefficient, Planck constant, light frequency, band gap energy and a constant, respectively. The plot of $(\alpha h\nu)^2$ *versus* $(h\nu)$ for nanoflower, nanospindle and nanorod are shown in Figure 4c. The band gap

energy (E_g)values of different nanostructures were calculated from the intercept of $(\alpha h\nu)^2$ *versus* $(h\nu)$ curves by extra-plotting tangent to them. The band gap of nanorod found to be 3.43 eV. However, the band gap decreased to 3.42 eV and 3.39 eV for nanospindle and nanoflower respectively (see figure 4c).

Photocatalytic performance

Photocatalytic properties for nanoflower, nanospindle and nanorod were evaluated by the decomposition of an anionic dye methyl orange (MO). The characteristic adsorption of MO was chosen at ~463 nm to monitor the photocatalytic degradation process.

The time dependent absorption spectra (Figure 4d) of MO aqueous solution were recorded during UV light irradiation in the presence of ZnO nanorod. A very slight decrease in the MO solution concentration was noticed, when the solutions were stirred for 30 minutes in dark to establish adsorption-desorption equilibrium of MO on the sample surface. It indicates that limited adsorption of MO is occurred on the samples surface after the adsorption-desorption equilibrium is set up. As a control, the absorbance peak of the MO solution was monitored without photocatalyst under UV light illumination. Insignificant change in the absorbance peak of MO under these conditions was observed demonstrating that there is no noticeable loss of MO concentration (figure 5a). When ZnO nanorod placed in an MO solution, the maximum absorption of the solution was found to decrease with irradiation time and color disappeared almost completely in 180 minutes. The photocatalytic performance ~50 % was achieved within 60 minutes irradiation of UV light, whereas after 180 minutes irradiation of UV light, ~89 % photocatalytic degradation of MO was occurred over ZnO nanorod. Further, in order to evaluate the relationship between photocatalysis and morphology, nanoflower and nanospindle were used as the contrast examples. The figure 5a shows the relative concentration (C/C_0) of MO versus irradiation time plots for various nanostructures, where C represents concentration of MO at the irradiation time (t) and C_0 is the concentration of the MO before irradiation. It was observed that concentration of the MO solution decrease with irradiation time for all ZnO nanostructures, indicating that all of the nanostructures show UV-light photocatalytic properties in the degradation of MO. The higher photocatalytic performance of ~89 % was achieved for nanorod within 180 minutes of photo-irradiation, whereas only ~80 % and ~69 % degradation capacity of MO was noticed with nanospindle and nanoflower, respectively (figure 5a). Therefore, it was observed that ZnO nanorod exhibited significantly higher photocatalytic activity for the photodegradation of MO than that of nanospindle and nanoflower.

To understand the kinetics behavior of these photocatalyst, the experimental data were fitted by following first-order reaction:

$$\ln(C_0/C) = Kt \qquad (2)$$

where K is the apparent rate constant (min^{-1}), t is the reaction time, C_0 and C are the concentration of MO dye at 0 and t, respectively. There is a linear relationship between $\ln(C_0/C)$ and the irradiation time for MO degradation as shown in figure 5(b). As evident from figure 5b, the photocatalytic degradation curves in all cases fit well with pseudo-first-order kinetics. The apparent reaction rate constant K for the photodegradation of MO was found to be 1.226×10^{-2} min^{-1}, 0.894×10^{-2} min^{-1} and 0.6689×10^{-2} min^{-1} for nanorod, nanospindle and nanoflower, respectively. The photocatalytic activity is directly related to the value of reaction rate constant. We observed that the reaction rate constant for nanorod is higher compared to nanoflower and nanospindle. This demonstrates the higher photocatalytic activities of ZnO nanorod. We found that the photocatalytic performance of the ZnO nanorod obtained in this study is comparatively better (even at low concentration) than other published reports[54-56]. This enhanced performance even at low concentration can be attributed to the absence of any capping ligand and or template in our reactions.

Stability and reusability of photocatalyst is important to reduce overall cost of photocatalysis process and strengthens practical utility. To evaluate the photocatalytic stability of the ZnO nanostructure photocatalysts, stability tests were conducted by executing recycling reactions five times for the photodegradation of MO under UV-vis light irradiation for nanorod. As shown in figure 5c, no noticeable loss of the photocatalytic activity of ZnO nanorod was observed for MO degradation reaction after repeated cycles. It indicates that ZnO nanorod have good stability and reusability performance and might be potent material for practical photocatalysis applications.

The UV light photodegradation mechanism of ZnO nanostructure photocatalysis is schematically illustrated in figure 5d. In the present work, ZnO nanorod show higher photocatalytic activity as compared to nanospindle and nanoflower. According to the references[57-59] several factor determine the photocatalytic activity of ZnO such as, active morphological surfaces, delay in recombination of electron-hole pairs and enhancement in adsorption of molecules on space charge region along the longitudinal direction of the nanorod. The enhanced oxygen adsorption on the surface of ZnO nanorod decreased the recombination probability of carriers by accepting photogenerated holes, which in turns forms reactive oxygen species and finally enhance the photocatalytic activity[60]. Probably, the formation rate of hydroxyl radical along the longitudinal surface of ZnO nanorod is high compared to nanospindle and nanoflower, owing to higher photocatalytic efficiency of nanorod.

Conclusions

In summary, we have studied the anion ligand effect of acetate and nitrate ions on the formation of different morphology of ZnO crystals in presence of NaOH and HMTA. We have varied the concentration of zinc salt precursors as well as adopted three different methods of synthesis (chemical, ultrasonic and

hydrothermal) to study their effects on the size/shape of the formed ZnO nanostructures. Results for each group where NaOH was used, suggests that morphology evolved to nanoflower, nanospindle, spherical aggregates and nanosheet-assembled flower-like ZnO nanostructures, which was ascribed to the process parameter and varying ratio of anions dependent tuning of the nanostructures. On the other hand, for each group where HMTA was used, morphology evolved in nanorod and semi-hollow nanorod of different aspect ratio, clearly demonstrating the dominance of HMTA. It is suggested that the presence of anions coming from zinc salts is a crucial factor for the morphologies of the obtained ZnO nanostructures. Such knowledge would allow laboratories and industries to rationally design experiments for anticipated morphology simply by selecting the appropriate zinc salt precursors. Furthermore, it is also suggested that role of other precursors salts in synergy will lead to formation of varied nanostructures and can be elaborated to other metal oxides of interest for modification. The photocatalytic properties of ZnO nanostructures (nanoflower, nanospindle and nanorod) towards MO under UV irradiation were found to be alluring. The enhanced percentage degradation of an anionic dye methyl orange with nanorod was found to be ~89% within three hours at very low concentration of ZnO nanorod (40 mg). Results show that rod like ZnO nanostructures are catalytically more reactive than nanoflower and nanospindle. These results also demonstrate that ZnO nanorod has good stability and reusability performance as photocatalyst.

Acknowledgements

The authors would like to thanks the National Research Foundation (NRF), South Africa and University of Johannesburg for financial support. The authors thank Dr. Ajay Mishra (Department of Applied Chemistry, University of Johannesburg) for useful discussions and suggestions.

Notes and references

[a] *Department of Applied Chemistry, University of Johannesburg, Doornfontein Campus, South Africa*

[b] *Department of Applied Physics and Engineering Mathematics, University of Johannesburg, Doornfontein Campus, South Africa*

† Morphologies of the ZnO nanostructures were studied using field emission scanning electron microscopy (TESCAN, VEGA SEM) under a 20 kV electron acceleration voltage coupled with an energy dispersive X-ray spectrum (EDS). The phase purity and crystal structure of the as prepared materials were investigated by X-Ray powder diffraction (XRD) using Rigaku Ultima IV, X-ray diffractometer at 40 kV and 40 mA with Cu-Kα radiation of the 0.15418 nm. The diffraction data were recorded for 2θ angles between 5° and 80° (step size: 0.02°, step time: 1min). All peak positions were indexed according to standard files to identify the crystalline phase. Raman spectrums were recorded in order to perform the phonon vibrational study of the ZnO nanostructures using micro-Raman spectrometer (NRS-3100) with a 532 nm solid-state primary laser as an excitation source in the backscattering configuration at room temperature. UV absorbance measurements were taken using Shimadzu UV-2450, UV-vis spectrophotometer in the range of 200-800 nm.

1. A. B. Djurišić, X. Chen, Y. H. Leung and A. M. C. Ng, J. Mater. Chem., 2012, 22, 6526.
2. P. Kumar, J. Singh, V. Parashar, K. Singh, R. S. Tiwari, O. N. Srivastava, K. Ramam and A. C. Pandey, *CrystEngComm*, 2012, **14** (5), 1653-1658
3. S. K. Pandey, S. Pandey, V. Parashar, R. S. Yadav, G. K. Mehrotra and A. C. Pandey, *Nanoscale*, 2014, **6** (3), 1602-1606
4. M. H. Huang, S. Mao, H. Feick, H. Yan, Y. Wu, H. Kind, E. Weber, R. Russo and P. Yang, *Science*, 2001, **292**, 1897.
5. N. Saito, H. Haneda, T. Sekiguchi, N. Ohashi, I. Sakaguchi and K. Koumoto, *Adv. Mater.*, 2002, **14**, 418.
6. Z. L. Wang and J. H. Song, *Science*, 2006, **312**, 242.
7. R. Ahmad, N. Tripathy, D. U. J. Jung and Y. B. Hahn, *Chem. Commun.*, 2014, **50**, 1890.
8. Y. Li, S. Li, L. Jin, J. B. Murowchick and Z. Peng, *RSC Adv.*, 2013, **3**, 16308.
9. X. Jiang, F. L. Wong, M. K. Fung and S. T. Lee, *Appl. Phys. Lett.*, 2003, **83**, 1875.
10. Y. Liu, J Shi, Q Peng and Y. Li, *J. Mater. Chem.*, 2012, **22**, 6539.
11. M. Raula, Md. H. Rashid, T. K. Paira, E. Dinda and T. K. Mandal, *Langmuir*, 2010, **26**, 8769.
12. M. Kirkham, Z. L. Wang and R. L. Snyder, *Nanotechnology*, 2008, **19**, 445708.
13. Y. Qiu, H. Zhang, L. Hu, D. Yang, L. Wang, B. Wang, J. Ji, G. Liu, X. Liu, J. Lin, F. Li and S. Han, *Nanoscale*, 2012, **4**, 6568.
14. V. Gaddam, R. R. Kumar, M. Parmar, G. R. K. Yaddanapudi, M. M. Nayak and K. Rajanna, *RSC Adv.*, 2015, **5**, 13519.
15. H. Yu, Z. Zhang, M. Han, X. Hao and F. Zhu, *J. Am. Chem. Soc.*, 2005, **127**, 2378.
16. P. Gao, Y. Chen, Y. Wang, Q. Zhang, X. Li and M. Hu, *Chem. Commun.*, 2009, 2762.
17. A. B. Djurišić, Y. H. Leung, W. C. H. Choy, K. W. Cheah and W. K. Chan, *Appl. Phys. Lett.*, 2004, **84**, 2635.
18. J. Zhang, L. Sun, J. Yin, H. Su, C. Liao and C. Yan, *Chem. Mater.*, 2002, **14**, 4172.
19. P. K. Baviskar, P. R. Nikam, S S. Gargote, A. Ennaoui, and B. R. Sankapal, *J. of Alloy and Compd.*, 2013, **551**, 233.
20. S. Cho, S. Kim, N. H. Kim, U. J. Lee, S. H. Jung, E. Oh and K. H. Lee, *J. Phys. Chem. C*, 2008, **112**, 17760.
21. W. S. Jang, T. I. Lee, J. Y. Oh, S. H. Hwang, S. W. Shon, Y. Xia, J. M. Myoung and H. K. Baik, *J. Mater. Chem.*, 2012, **22**, 20719.
22. P. S. Venkatesh and K. Jeganathan, *CrystEngComm*, 2014, **16**, 7426.
23. S. P. Garcia and S. Semancik, *Chem. Mater.* 2007, **19**, 4016.
24. T. L. Sounart, J. Liu, J. A. Voigt, M. Huo, E. D. Spoerke and B. Mckenzie, *J. Am. Chem. Soc.* 2007, **129**, 15786.
25. L. F. Xu, Y. Guo, Q. Liao, J. P. Zhang and D. S. Xu, *J. Phys. Chem. B*, 2005, **109**, 13519.
26. J. Du, Z. Liu, Y. Huang, Y. Gao, B. Han, W. Li and G. Yang, *J. Cryst. Growth*, 2005, **280**, 126.

27. A. Taubert, D. Palms, O. Weiss, M. T. Piccini and D. N. Batchelder, *Chem. Mater.*, 2002, **14**, 2594.
28. Y. Liu, K. Tai, and S. J. Dillon, *Chem. Mater.*, 2013, **25**, 2927.
29. M. H. Rashid, M. Raula, R. R. Bhattacharjee and T. K. Mandal, *J. Colloid Interface Sci.*, 2009, **339**, 249–258.
30. A. Taubert, G. Glasser and D. Palms, *Langmuir*, 2002, **18**, 4488.
31. H. Zhang, D. Yang, D. Li, X. Ma, S. Li and D. Que, *Cryst. Growth Des.* 2005, **5**, 547.
32. M. Umetsu, M. Mizuta, K. Tsumoto, S. Ohara, S. Takami, H. Watanabe, I. Kumagai and T. Adschiri, *Adv. Mater.*, 2005, **17**, 2571.
33. R. Ullah and J. Dutta, *J. Hazard. Mater.*, 2008, **156**, 194.
34. S. Banerjee, S. C. Pillai, P. Falaras, K. E. O'Shea, J. A. Byrne and D. D. Dionysiou, *J. Phys. Chem. Lett.*, 2014, **5**, 2543.
35. Y. Zheng, C. Chen, Y. Zhan, X. Lin, Qi Zheng, Kemei Wei, J. Zhu and Y. Zhu, *Inorg. Chem.*, 2007, **46**, 6675.
36. L. N. Demianets, D. V. Kostomarov, I. P. Kuz'mina and S. V. Pushko, *Crystallogr. Rep.*, 2002, **47**, S86.
37. R. Viswanatha, H. Amenitsch and D. D. Sarma, *J. Am. Chem. Soc.*, 2007, **129**, 4470.
38. J. Song, S. Baek, J. Lee and S. Lim, *Chem. Tech. and Biotech.*, 2008, **83**, 345.
39. K. Fujita, K. Murata, T. Nakazawa and I. Kayama, *Yogyo Kyokaishi*, 1984, **92**, 227.
40. A. Sugunan, H. C. Warad, M. Boman and J. Dutta, *J. Sol-Gel Sci. Technol.*, 2006, **39**, 49.
41. K. M. McPeak, T. P. Le, N. G. Britton, Z. S. Nickolov, Y. A. Elabd and J. B. Baxter, *Langmuir* 2011, **27**, 3672.
42. V. Strano, R. G. Urso, M. Scuderi, K. O. Iwu, F. Simone, E. Ciliberto, C. Spinella and S. Mirabella, *J. Phys. Chem. C*, 2014, **118**, 28189.
43. C. Tamuly, I. Saikia, M. Hazarika, M. Bordoloi, N. Hussain, M. R. Dasc and K. Deka, *RSC Adv.*, 2015, **5**, 8604.
44. Y. Inubushi, R. Takami, M. Iwasaki, H. Tada and S. Ito, *J. Colloid Interface Sci.*, 1998, **200**, 220.
45. A. R. Abbasi and A. Morsali, *UItrason. Sonochem*, 2010, **17**, 704.
46. H. J. Fan, A. S. Barnard and M. Zacharias, *Appl. Phys. Lett.*, 2007, **90**, 143116.
47. B. Liu and H. Zeng, *Langmuir*, 2004, **20**, 4196.
48. Y. Peng, A. W. Xu, B. Deng, M. Antonietti and H. Cölfen, *J. Phys. Chem. B*, 2006, **110**, 2988.
49. D. Wang, Y. Zhao and C. Song, *Solid States Sci.*, 2010, **12**, 776.
50. Q. Liu, L. Jiang and L. Guo, *Small*, 2014, **10**, 48.
51. R. Sato-Berru, Y. A.V´azquez-Olmos, A. L. Fern´andez-Osorio and S. Sotres-Mart´ınez, *J. Raman Spectrosc.*, 2007, **38**, 1073.
52. G. D. Nagy and E. J. Casey, *John Wiley & Sons: New York*, 1971, 133.
53. J. I. Pankove, *Prentice-Hall Inc., Englewoord Cliffs, NJ*, 1971.
54. S. Danwittayakul, M. Jaisai, T. Koottatep and J. Dutta, *Ind. Eng. Chem. Res.*, 2013, **52**, 13629.
55. L.A. Ghule, A.A. Patil, K.B. Sapnar, S.D. Dhole and K.M. Garadkar, 2011, **93**, 623.
56. J. X. Sun, Y. P. Yuan, L. G. Qiu, X. Jiang, A. J. Xie, Y. H. Shen and J. F. Zhu, *Dalton Trans.*, 2012, **41**, 6756.
57. D. Li, R. Shi, C. Pan, Y. Zhu and H. Zhao, *CrystEngComm*, 2011, **13**, 4695.
58. J. Chang and E. R. Waclawik, *CrystEngComm*, 2012, **14**, 4041.
59. H. J. Yun, H. Lee, J. B. Joo, W. Kim and J. Yi, *J. Phys. Chem. C*, 2009, **113**, 3050.
60. L. S. Zhang, K. H. Wong, D. Q. Zhang, C. Hu, J. C. Yu, C. Y. Chan and P. K. Wong, *Environ. Sci. Technol.*, 2009, **43**, 7883.